Annals of Glaciology

Article

Cite this article: Haynes MS (2020). Surface and subsurface radar equations for radar sounders. *Annals of Glaciology* **61**(81), 135–142. https://doi.org/10.1017/aog.2020.16

Received: 26 November 2019
Revised: 17 March 2020
Accepted: 19 March 2020
First published online: 24 April 2020

Author for correspondence:
Mark Haynes,
E-mail: mark.s.haynes@jpl.nasa.gov

cambridge.org/aog

Surface and subsurface radar equations for radar sounders

Mark S. Haynes

Jet Propulsion Laboratory, California Institute of Technology, Pasadena, CA, USA

Abstract

This work is a collection of radar equations for low-frequency radar sounding and radar in general that emphasize the form of the radar equation for different target and source geometries. This is meant as a handbook for scientists and engineers that work with or analyze radar sounder systems and interpret radar sounding echoes. Lookup tables summarize the results and derivations are provided for each equation.

1. Introduction

Low-frequency radar sounders (e.g, HF, VHF) have been used for decades to probe ice-sheets and subsurfaces for both terrestrial and planetary science investigations. They are nadir pointing radar systems that have wide along-track and cross-track beam patterns. Terrestrial airborne sounders include High-Capability Radar Sounder (HiCARS), Multichannel Coherent Radar Depth Sounder (MCoRDS), Polarimetric Airborne Survey Instrument (PASIN) and Polarimetric Airborne Radar Ice Sounder (POLARIS) (Peters and others, 2005, 2007; Hélière and other, 2007; Shi and others, 2010; Karlsson and other, 2009; Dall and others, 2010; Rodriguez-Morales and others, 2013). Planetary sounders include Mars Advanced Radar for Subsurface and Ionospheric Sounding (MARSIS), Shallow Radar (SHARAD) and Lunar Radar Sounder (LRS) (Picardi and others, 2004; Seu and others, 2007; Ono and Oya, 2000), as well as Radar for Europa Assessment and Sounding: Ocean to Near-surface (REASON) and Radar for Icy Moon Exploration (RIME), (Blankenship and other, 2009; Moussessian, 2015; Bruzzone and others, 2013), which are currently being developed.

The choice of radar equation for radar sounding analysis, and radar in general, has important implications for system link budgets and scientific interpretation of radar echoes. While there is one fundamental radar equation, it will take different forms depending on the properties of the target and source geometry. These forms elucidate different aspects of the problem and highlight sensitivity to certain parameters, such as the exponent of the geometric power fall-off or the origin of certain multiplying constants. For example, there is a 10 dB swing between the radar equation derived for a flat surface Fresnel zone with plane wave incidence and the radar equation derived using the image method (Haynes and others, 2018). Another example is geometric spreading losses that must be corrected when estimating absolute surface or basal reflectivity, and in the case of high-altitude planetary sounders, the use of flat or spherical surface assumptions can change this correction by several dB. It is up to the practitioner to choose the radar equation that is most appropriate for their problem. The wide variety of possible target and source geometries that need to be considered when doing system analysis or interpreting echoes is the central motivation for compiling the tables that follow.

This work is a collection of radar equations for the analysis of low-frequency radar sounding systems, and radar systems in general. The purpose is to serve as a handbook for scientists and engineers to quickly look up these equations, assumptions and derivations. Emphasis is placed on the form of the radar equation under different sensor and target geometries, rather than the details of radar system hardware, signal processing or scattering phenomenology. Many of these equations appear in textbooks and throughout the literature (Gudmandsen, 1971; Ulaby and others, 1982; Chyba and others, 1998; Biccari and other, 2001; Picardi and others, 2004; Peters and others, 2005; Ulaby and others, 2014; Haynes and others, 2018), but a central collection does not exist and several new variants are included here. This is meant as a starting point for comparison, system analysis and scientific interpretation of radar echoes and builds on the results in Haynes and others (2018).

The geometries for which radar equations are derived and tabulated here are combinations of, but not limited to:

1. active/passive radar sounding
2. Fresnel-zone/pulse-limited target area
3. surface/subsurface interfaces
4. flat/spherical surfaces
5. spherical-wave/plane-wave incidence
6. monostatic/bistatic source and receiver configurations

Most geometries are for normal incidence over a homogeneous medium, with special attention to Fresnel-zone sized targets. Several off-nadir geometries are included, as well as a section

Table 1. Table of symbols

Symbol	Description
R, r_1, r_2	Sensor range
h, h_1, h_2	Sensor nadir altitude
r	Spherical body radius
d	Subsurface interface depth
λ, λ_{ϵ_r}	Wavelength in free-space or dielectric medium
k	Wavenumber
Γ	Reflectivity at an interface
T	Transmissivity at an interface
P_t	Radar transmit power
S	Plane wave power density
G_t, G_r	Transmitter/Receiver antenna gain
A_r	Effective aperture of receive antenna
n	Index of refraction
ϵ_r	Relative permittivity
σ, σ_{ϵ_r}	Radar cross-section in free-space or dielectric medium
σ_o, σ_{o,ϵ_r}	Normalized radar cross-section in free-space or dielectric medium
g_r, g_r'	Refraction gain for nadir or off-nadir geometry
$\Delta\rho$	Radar slant-range resolution
r_f, r_p	Fresnel zone radius or pulse limited radius
a, b	Fresnel zone ellipse parameters
θ_i, θ_t	Incidence and transmission angles

on bistatic geometries and bistatic Fresnel zones, which is included for general reference and to show how the bistatic expressions reduce to the simpler cases in the right limits. Finally, geometries for passive radar sounding, which uses astronomical or natural radio sources in place of a transmitter (Cecconi and others, 2012; Romero-Wolf and others, 2015; Schroeder and others, 2016; Peters and others, 2018), are included as well. In passive sounding, the incidence field is truly planar, which has interesting consequences for its radar equations.

Section 2 contains lookup tables that summarize the results. Each table row includes a short description of the geometry, a graphical representation of the geometry, the equation and citation, as well as the section and equation numbers in the Supplementary Material where derivations can be found. New variants, or those for which citations were not readily found, are noted with ***. Derivations rely largely on image methods, large-argument approximations, small-angle approximations and scalar surface phase integrals under the assumption of Kirchhoff scattering. Observations, recommendations and commentary are included throughout the derivations to help draw attention to notable connections between results.

While the primary application is low-frequency radar sounding, the equations are general enough that the user can augment these for their particular problem and radar system. The list is not exhaustive, and more advanced variants and combinations exist and can be derived, for instance expressions that contain integrals over angle-dependent antenna beam patterns or scattering functions.

The organization of the paper is as follows: Section 1.1 has a list of assumptions and conventions used throughout the work and which help to use the tables. Section 2 contains the lookup tables, including one for Fresnel zone radius. Derivations can be found in the Supplementary Material: Section S1 contains the derivations for surface geometries. Section S2 covers subsurface geometries. Section S3 covers pulse limited surface and subsurface geometries. Section S4 covers passive radar sounding for surface targets. Finally, Section S5 contains derivations for bistatic geometries and bistatic Fresnel zones.

1.1. Using the tables

The following assumptions and conventions apply to the radar equations, geometries and derivations that are summarized in the tables in Section 2:

1. Radar equations give single-pulse raw received power. Processing gains, synthetic aperture radar (SAR) resolution target area and system losses are not included.
2. Distances between sensors and targets are assumed large compared to the wavelength. Most derivations rely on large-argument/small-angle approximations.
3. All expressions for Fresnel zone radius, r_f, in the table are approximations.
4. The medium above the surface interface is assumed to be free-space.
5. Angular dependence and polarization of backscatter, antenna gain, reflectivity or transmissivity are suppressed for clarity.
6. Subsurface media are assumed lossless. Propagation losses can be included as needed.
7. Interfaces to which reflectivity, Γ, and transmissivity, T, apply should be understood in context.
8. Surface phase integrals implicitly start from the assumption of Kirchhoff scattering.
9. Any occurrence of reflectivity, Γ, and transmissivity, T, can be augmented with higher-fidelity scattering models that are proportional to reflectivity or transmissivity. For example, the exponential form of coherence loss derived under the Kirchhoff approximation for small-roughness can be included at any interface.
10. Transmitter and receiver gain, G_t and G_r, are notated separately, rather than G^2, to accommodate bistatic geometries or systems that transmit and receive from different, but possibly co-located, antennas.

https://doi.org/10.1017/aog.2020.16 Published online by Cambridge University Press

2. Tables of radar equations and fresnel zone radius

In all tables, subsurface is indicated with grey shading in the column Geometry, and new variants of equations, or those for which citations were not readily found, are noted with *** in the column Citation.

Table 2. Active sounding – surface

Description	Geometry	Equation	Eq. No.	Citation
Basic radar equation Sec. S1.1	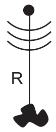	$P_r = \frac{P_t G_t G_r \lambda^2 \sigma}{(4\pi)^3 R^4}$	(S.1)	(Ulaby and others, 1982, 2014)
Image method Spherical waves Flat surface Sec.S1.2	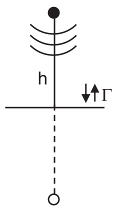	$P_r = \frac{P_t G_t G_r \lambda^2 \Gamma}{(4\pi)^2 (2h)^2}$	(S.9)	(Ulaby and others, 2014; Nguyen and Park, 2016; Moore and Williams, 1957; Edison and others, 1960; Fung and Eom, 1983)
Fresnel zone Spherical waves Flat surface Sec. S1.4	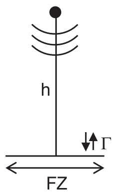	$P_r = \frac{P_t G_t G_r \lambda^2 \Gamma}{(4\pi)^2 h^2}$	(S.28)	(Haynes and others, 2018)
Fresnel zone Spherical waves Spherical surface Sec. S1.5	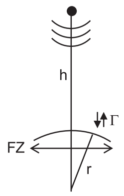	$P_r = \frac{P_t G_t G_r \lambda^2 \Gamma}{(4\pi)^2 h^2} \frac{r^2}{(h+r)^2}$	(S.56)	(Haynes and others, 2018)
Fresnel zone Plane waves 'Antenna' approach Flat surface Sec. S1.6	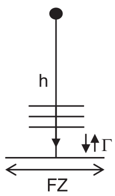	$P_r = \frac{P_t G_t G_r \lambda^2 \Gamma}{4^3 h^2}$	(S.60)	(Haynes and others, 2018)

Table 3. Active sounding – subsurface

Description	Geometry	Equation	Eq. No.	Citation
Subsurface Image method Spherical waves Flat surface Flat subsurface Sec. S2.1	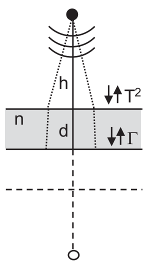	$P_r = \frac{P_t G_t G_r \lambda^2 T^2 \Gamma}{(4\pi)^2 (2(h+d))^2} g_r^2$	S.73	(Gudmandsen, 1971; Chyba and others, 1998; Peters and others, 2005; Kofman and others, 2010)
Subsurface 1-way refraction gain Flat surface Sec. S2.2	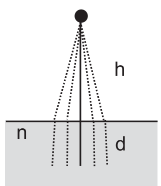	$g_r = \frac{h+d}{h+d/n}$	S.75	(Gudmandsen, 1971)

(*Continued*)

https://doi.org/10.1017/aog.2020.16 Published online by Cambridge University Press

Table 3. (*Continued.*)

Description	Geometry	Equation	Eq. No.	Citation
Subsurface nadir General radar equation Spherical waves Flat surface Sec. *S*2.3	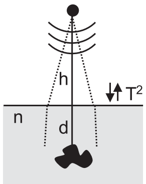	$P_r = \frac{P_t G_t G_r \lambda^2 T^2 \sigma_{\epsilon_r}}{(4\pi)^3 (h+d)^4} \frac{g_r^4}{n^2}$	S.98	(Peters and others, 2005)
Subsurface off-nadir General radar equation Spherical waves Flat surface Sec. *S*2.4	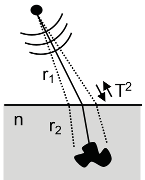	$P_r = \frac{P_t G_t G_r \lambda^2 T^2 \sigma_{\epsilon_r}}{(4\pi)^3 (r_1+r_2)^4} \frac{g_r'^4}{n^2}$	S.124	***
Subsurface Fresnel zone Spherical waves Flat surface Flat subsurface Sec. *S*2.5	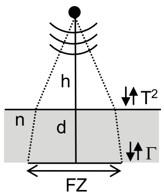	$P_r = \frac{P_t G_t G_r \lambda^2 T^2 \Gamma}{(4\pi)^2 (h+d)^2} g_r^2$	S.159	***
Subsurface Fresnel zone Plane waves Flat surface Flat subsurface Sec. *S*2.6	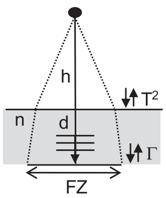	$P_r = \frac{P_t G_t G_r \lambda^2 T^2 \Gamma}{4^3 (h+d)^2} g_r^2$	S.166	***
Subsurface Fresnel zone Spherical waves Flat surface Spherical subsurface Sec. *S*2.7	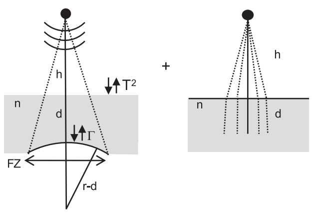	$P_r = \frac{P_t G_t G_r \lambda^2 T^2 \Gamma}{(4\pi)^2 (h+d)^2} g_r^2 \cdot \frac{(r-d)^2}{((r-d)+(h+d))^2}$	S.210	***
Subsurface Fresnel zone Spherical waves Spherical surface Spherical subsurface Sec. *S*2.7	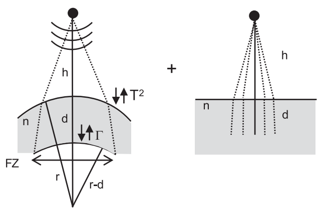	$P_r = \frac{P_t G_t G_r \lambda^2 T^2 \Gamma}{(4\pi)^2 (h+d)^2} g_r^2 \cdot \frac{(r-d)^2}{((r-d)+(h+d))^2} \cdot \left(\frac{r(r+h)n(h+d/n)}{hn(r-d)(r+h)+d(hn+r)^2} \right)^2$	S.209	***

Table 4. Pulse limited

Description	Geometry	Equation	Eq. No.	Citation
Pulse limited Spherical waves Flat surface Sec. *S*3.1	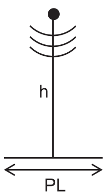	$P_r = \frac{P_t G_t G_r \lambda^2 \sigma_o \Delta\rho}{2^5 \pi^2 h^3}$	S.213	(Moore and Williams, 1957; Ulaby and others, 2014; Haynes and others, 2018)
Pulse limited Spherical waves Spherical surface Sec. *S*3.2	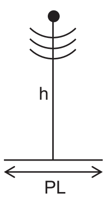	$P_r = \frac{P_t G_t G_r \lambda^2 \sigma_o \Delta\rho}{2^5 \pi^2 h^3} \frac{r}{h+r}$	S.215	***

(*Continued*)

https://doi.org/10.1017/aog.2020.16 Published online by Cambridge University Press

Table 4. (*Continued.*)

Description	Geometry	Equation	Eq. No.	Citation
Pulse limited Spherical waves Flat surface Flat subsurface Sec. *S*3.3	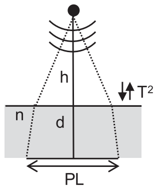	$P_r = \frac{P_t G_t G_r \lambda^2 T^2}{2^5 \pi^2 (h+d)^3} g_r^3 \frac{\sigma_{o,\epsilon_r} \Delta\rho}{n^2}$	S.220	***
Pulse limited Spherical waves Flat surface Spherical subsurface Sec. *S*3.4	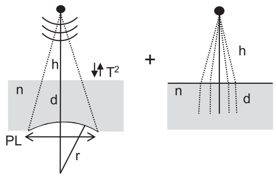	$P_r = \frac{P_t G_t G_r \lambda^2 T^2}{2^5 \pi^2 (h+d)^3} g_r^3 \frac{\sigma_{o,\epsilon_r} \Delta\rho}{n^2} \cdot \frac{(r-d)}{(h+d)+(r-d)}$	S.221	***

Table 5. Passive sounding

Description	Geometry	Equation	Eq. No.	Citation
Passive radar equations Sec. *S*4.1	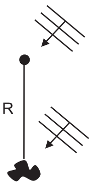	$P_d = \frac{S G_d \lambda^2}{4\pi}$ $P_r = \frac{S G_r \lambda^2 \sigma}{(4\pi)^2 R^2}$	S.222 S.223	***
Passive Fresnel zone Normal plane wave incidence Spherical scattering Flat surface Sec. *S*4.2	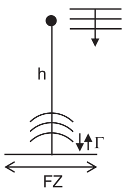	$P_r = \frac{S G_r \lambda^2 \Gamma}{\pi}$	S.235	***
Passive Fresnel zone Normal plane wave incidence Plane wave scattering Flat surface Sec. *S*4.3	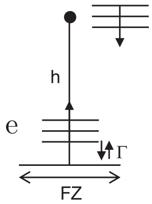	$P_r = \frac{S G_r \lambda^2 \Gamma \pi}{4}$	S.239	***
Passive Fresnel zone Normal plane wave incidence Spherical scattering Spherical surface Sec. *S*4.4	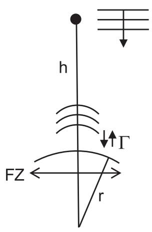	$P_r = \frac{S G_r \lambda^2 \Gamma}{\pi} \frac{r^2}{(2h+r)^2}$	S.265	***
Passive Fresnel zone Off-nadir plane wave incidence Spherical scattering Flat surface Sec. *S*4.5	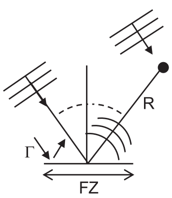	$P_r = \frac{S G_r \lambda^2 \Gamma}{\pi}$	S.271	***

https://doi.org/10.1017/aog.2020.16 Published online by Cambridge University Press

Table 6. Bistatic

Description	Geometry	Equation	Eq. No.	Citation
Bistatic radar equation Sec. *S*5.1	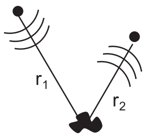	$P_r = \frac{P_t G_t G_r \lambda^2 \sigma}{(4\pi)^3 r_1^2 r_2^2}$	S.272	(Ulaby and others, 2014; Hajj and Zuffada, 2003)
Bistatic Image method Spherical waves Flat surface Sec. *S*5.2	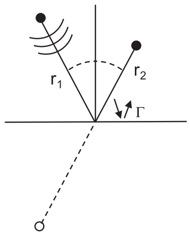	$P_r = \frac{P_t G_t G_r \lambda^2 \Gamma}{(4\pi)^2 (r_1 + r_2)^2}$	S.278	(Ulaby and others, 2014; Carreno-Luengo and others, 2018)
Bistatic Fresnel zone Spherical waves Flat surface Sec. *S*5.6	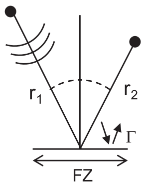	$P_r = \frac{P_t G_t G_r \lambda^2 \Gamma}{4\pi^2 (r_1 + r_2)^2}$	S.355	***
Bistatic Fresnel zone Plane waves Flat surface Sec. *S*5.7	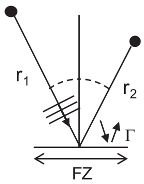	$P_r = \frac{P_t G_t G_r \lambda^2 \Gamma}{4^2 (r_1 + r_2)^2}$	S.358	***
Bistatic Fresnel zone Spherical waves Spherical surface Sec. *S*5.8	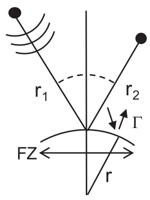	$P_r = \frac{P_t G_t G_r \Gamma}{4\pi^2 r_1^2 r_2^2} a^2 b^2 \cos^2 \theta_i$	S.377	***
Bistatic Subsurface receiver Flat surface Sec. *S*5.9	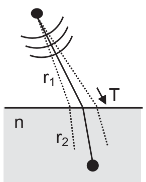	$P_r = \frac{P_t G_t G_r \lambda^2 T}{(4\pi)^2 (r_1 + r_2)^2} \frac{g_r'^2 \cos \theta_i}{n^2 \cos \theta_t}$	S.381	***

Table 7. Fresnel zone radius

Description	Geometry	Equation	Eq. No.	Citation
Flat surface	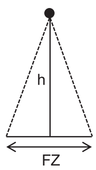	$r_f = \sqrt{\frac{\lambda h}{2}}$	S.21	(Seu and others, 2007; Bruzzone and others, 2011; Schroeder and others, 2016; Haynes and others, 2018)
Spherical surface	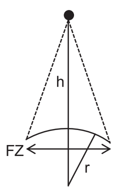	$r_f = \sqrt{\frac{\lambda h r}{2(h + r)}}$	S.46	(Haynes and others, 2018)

(*Continued*)

https://doi.org/10.1017/aog.2020.16 Published online by Cambridge University Press

Table 7. (*Continued.*)

Description	Geometry	Equation	Eq. No.	Citation
Flat surface Flat subsurface	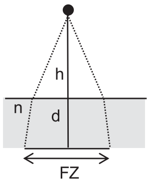	$r_f = \sqrt{\frac{\lambda}{2}(h+\frac{d}{n})}$	S.153	(Peters and others, 2005)
Spherical surface Spherical subsurface	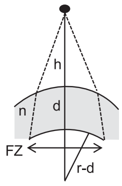	$r_f = \sqrt{\frac{\lambda}{2}(h+\frac{d}{n})} \cdot \sqrt{\frac{nr(r-d)(h+d/n)}{hn(r-d)(r+h)+d(hn+r)^2}}$	S.187	***
Bistatic Normal incidence Flat surface	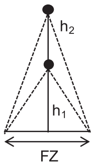	$r_f = \sqrt{\frac{\lambda h_1 h_2}{h_1+h_2}}$	S.302	(Schroeder and others, 2016)
Bistatic Normal incidence Spherical surface	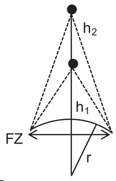	$r_f = \sqrt{\frac{\lambda r h_1 h_2}{r(h_1+h_2)+2h_1 h_2}}$	S.326	***
Bistatic specular Fresnel zone ellipse Flat surface	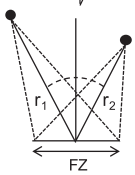	$a^2 = \frac{b^2}{\cos^2\theta_i}$ $b^2 = \frac{\lambda r_1 r_2}{r_1+r_2}$	S.296 S.297	(Hajj and Zuffada, 2003)
Bistatic specular Fresnel zone ellipse Spherical surface	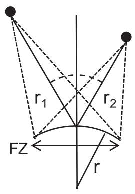	$a^2 = \left[\frac{r_1+r_2}{\lambda r_1 r_2}\cos^2\theta_i + \frac{2}{\lambda r}\cos\theta_i\right]^{-1}$ $b^2 = \left[\frac{r_1+r_2}{\lambda r_1 r_2} + \frac{2}{\lambda r}\cos\theta_i\right]^{-1}$	S.319 S.320	***
Passive Normal plane wave incidence Flat surface	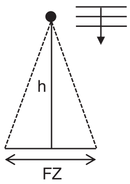	$r_f = \sqrt{\frac{\lambda}{2}(2h)}$	S.231	(Schroeder and others, 2016)
Passive Normal plane wave incidence Spherical surface	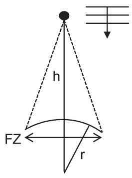	$r_f = \sqrt{\frac{\lambda}{2}\frac{(2h)r}{(2h)+r}}$	S.259	(Romero-Wolf and others, 2015)
Passive Fresnel zone ellipse Off – nadir incidence Flat surface	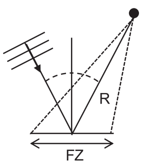	$a^2 = \frac{b^2}{\cos^2\theta_i}$ $b^2 = \lambda R$	S.266 S.267	***

https://doi.org/10.1017/aog.2020.16 Published online by Cambridge University Press

Supplementary material. The supplementary material for this article can be found at https://doi.org/10.1017/aog.2020.16.

Acknowledgments. The author thanks several people who contributed generous time and energy to carefully reading, editing and checking this work, which has greatly improved its substance, presentation and usefulness. Ilgin Seker (JPL) for reading a first draft and providing several insights; Dragana Perkovic-Martin (JPL) for reviewing an early draft; Dustin Schroeder (Stanford) for encouraging its publication as well as participation from his students: Riley Culberg (Stanford), Anna Broome (Stanford), Nicole Bienert (Stanford) and Sean Peters (Stanford), who each contributed numerous valuable suggestions and corrections, both detailed and nuanced, on content, style, references, table entries and figures. The author would also like to thank the two anonymous reviewers for their careful reading of the work and helpful improvements.

The research was carried out at the Jet Propulsion Laboratory, California Institute of Technology, under a contract with the National Aeronautics and Space Administration. This work was supported in part by the Europa Clipper Project. Government sponsorship acknowledged.

References

Biccari D, Picardi G, Seu R and Melacci P (2001) Mars surface models and subsurface detection performance in MARSIS. In Geoscience and Remote Sensing Symposium, 2001. IGARSS'01. IEEE 2001 International, Sydney, Australia, **6**, 2560–2562. IEEE. doi:10.1109/IGARSS.2001.978088

Blankenship DD, Young DA, Moore WB and Moore JC (2009) *Radar Sounding of Europa's Subsurface Properties and Processes: The View from Earth*. Tucson, AZ: Europa University of Arizona Press.

Brown G (1977) The average impulse response of a rough surface and its applications. *IEEE Transactions on antennas and Propagation* **25**(1), 67–74. doi:10.1109/JOE.1977.1145328

Bruzzone L and 5 others (2011) Subsurface radar sounding of the Jovian moon Ganymede. *Proceedings of the IEEE* **99**(5), 837–857.

Bruzzone L and 9 others (2013) RIME: Radar for icy moon exploration. In Geoscience and Remote Sensing Symposium (IGARSS), 2013 IEEE International, Melbourne, Australia, pages 3907–3910. IEEE. doi:10.1109/IGARSS.2013.6723686

Carreno-Luengo H, Luzi G and Crosetto M (2018) Sensitivity of CYGNSS bistatic reflectivity and SMAP microwave radiometry brightness temperature to geophysical parameters over land surfaces. *IEEE Journal of Selected Topics in Applied Earth Observations and Remote Sensing* **12**(1), 107–122. doi:10.1109/JSTARS.2018.2856588.

Cecconi B and 9 others (2012) Natural radio emission of Jupiter as interferences for radar investigations of the icy satellites of Jupiter. *Planetary and Space Science* **61**(1), 32–45. doi:10.1016/j.pss.2011.06.012.

Chyba CF, Ostro SJ and Edwards BC (1998) Radar detectability of a subsurface ocean on Europa. *Icarus* **134**(2), 292–302. doi:10.1006/icar.1998.5961.

Dall J and 9 others (2010) ESA's polarimetric airborne radar ice sounder (POLARIS): design and first results. *IET Radar, Sonar & Navigation* **4**(3), 488–496. doi:10.1049/iet-rsn.2009.0035.

Edison A, Moore R and Warner B (1960) Radar terrain return measured at near-vertical incidence. *IRE Transactions on Antennas and Propagation* **8**(3), 246–254. doi:10.1109/TAP.1960.1144843.

Fung A and Eom H (1983) Coherent scattering of a spherical wave from an irregular surface. *IEEE Transactions on Antennas and Propagation* **31**(1), 68–72. doi:10.1109/TAP.1983.1142979.

Gudmandsen P (1971) Electromagnetic probing of ice. In Wait JR ed. *Electromagnetic probing in geophysics*, Boulder, Colorado: Golem Press, 321.

Hajj GA and Zuffada C (2003) Theoretical description of a bistatic system for ocean altimetry using the GPS signal. *Radio Science* **38**(5), 1–10. doi: 10.1029/2002RS002787.

Hayne G (1980) Radar altimeter mean return waveforms from near-normal-incidence ocean surface scattering. *IEEE Transactions on Antennas and Propagation* **28**(5), 687–692. doi:10.1109/TAP.1980.1142398.

Haynes MS, Chapin E and Schroeder DM (2018) Geometric power fall-off in radar sounding. *IEEE Transactions on Geoscience and Remote Sensing* **56**(11), 6571–6585. doi:10.1109/TGRS.2018.2840511.

Hélière F, Lin CC, Corr H and Vaughan D (2007) Radio echo sounding of pine island glacier, west antarctica: aperture synthesis processing and analysis of feasibility from space. *IEEE Transactions on Geoscience and Remote Sensing* **45**(8), 2573–2582. doi:10.1109/TGRS.2007.897433.

Karlsson NB, Rippin DM, Vaughan DG and Corr HF (2009) The internal layering of Pine Island Glacier, West Antarctica, from airborne radar-sounding data. *Annals of Glaciology* **50**(51), 141–146. doi:10.3189/S0260305500250660.

Kofman W, Orosei R and Pettinelli E (2010) Radar signal propagation and detection through ice. *Space science reviews* **153**(1-4), 249–271. doi:10.1007/s11214-010-9642-2.

Kong J (1986) *Electromagnetic Wave Theory*. Wiley: A Wiley-Interscience publication.

Levine D (1984) The radar cross section of dielectric disks. *IEEE transactions on antennas and propagation* **32**(1), 6–12. doi:10.1109/TAP.1984.1143180.

Moore RK and Williams C (1957) Radar terrain return at near-vertical incidence. *Proceedings of the IRE* **45**(2), 228–238. doi:10.1109/JRPROC.1957.278394.

Moussessian A (2015) REASON for Europa. In *2015 AGU Fall Meeting*, AGU.

Nguyen C and Park J (2016) *Stepped-frequency Radar Sensors: Theory, Analysis and Design*. AG, Switzerland: Springer.

Ono T and Oya H (2000) Lunar Radar Sounder (LRS) experiment on-board the SELENE spacecraft. *Earth, planets and space* **52**(9), 629–637. doi:10.1186/BF03351671.

Patterson G and 13 others (2017) Bistatic radar observations of the Moon using Mini-RF on LRO and the Arecibo Observatory. *Icarus* **283**, 2–19. doi: 10.1016/j.icarus.2016.05.017.

Peters ME and 5 others (2007) Along-track focusing of airborne radar sounding data from west antarctica for improving basal reflection analysis and layer detection. *IEEE Transactions on Geoscience and Remote Sensing* **45**(9), 2725–2736. doi:10.1109/TGRS.2007.897416.

Peters ME, Blankenship DD and Morse DL (2005) Analysis techniques for coherent airborne radar sounding: application to west antarctic ice streams. *Journal of Geophysical Research: Solid Earth* **110**(B6), 1–17. doi: 10.1029/2004JB003222.

Peters ST, Schroeder DM, Castelletti D, Haynes M and Romero-Wolf A (2018) In situ demonstration of a passive radio sounding approach using the Sun for echo detection. *IEEE Transactions on Geoscience and Remote Sensing* **56**(12), 7338–7349. doi:10.1109/TGRS.2018.2850662.

Picardi G and 9 others (2004a) Performance and surface scattering models for the Mars Advanced Radar for Subsurface and Ionosphere Sounding (MARSIS). *Planetary and Space Science* **52**(1), 149–156. doi:10.1016/j.pss.2003.08.020.

Picardi G and 9 others (2004b) MARSIS: Mars advanced radar for subsurface and ionosphere sounding. Wilson A and Chicarro A eds. *Mars Express: The Scientific Payload*. ESA SP-1240. Noordwijk, Netherlands: ESA Publications Division, 51–69.

Rodriguez-Morales F and 9 others (2013) Advanced multifrequency radar instrumentation for polar research. *IEEE Transactions on Geoscience and Remote Sensing* **52**(5), 2824–2842. doi:10.1109/TGRS.2013.2266415.

Romero-Wolf A and 5 others (2015) A passive probe for subsurface oceans and liquid water in Jupiter's icy moons. *Icarus* **248**, 463–477. doi:10.1016/j.icarus.2014.10.043.

Schroeder DM and 7 others (2016) Assessing the potential for passive radio sounding of Europa and Ganymede with RIME and REASON. *Planetary and Space Science* **134**, 52–60. doi:10.1016/j.pss.2016.10.007.

Seu R and 9 others (2007) SHARAD sounding radar on the Mars Reconnaissance Orbiter. *Journal of Geophysical Research: Planets* **112**(E5), 1–18. doi: 10.1029/2006JE002745.

Shi L and 8 others (2010) Multichannel coherent radar depth sounder for NASA Operation Ice Bridge. In Geoscience and Remote Sensing Symposium (IGARSS), 2010 IEEE International, Honolulu, Hawaii, pages 1729–1732. IEEE. doi:10.1109/IGARSS.2010.5649518

Tsang L, Kong J and Ding K (2000) Scattering of electromagnetic waves, vol. 1: Theory and applications.

Ulaby FT and 8 others (2014) *Microwave radar and radiometric remote sensing*. Vol. 4. Ann Arbor: University of Michigan Press.

Ulaby F, Moore R and Fung A (1982) Microwave remote sensing: active and passive. volume 2-radar remote sensing and surface scattering and emission theory.